TECHNISCHE UNIVERSITÄT WIEN

Diplomarbeit

A Nanocrystalline Sensor for Local Induction Measurements in Laminated Machine Cores

ausgeführt zum Zwecke der Erlangung
des Akademischen Grades eines Diplom-Ingenieurs

Betreuer:

Univ.Prof. Dipl.-Ing. Dr.techn. Helmut Pfützner
Dipl.-Ing. Dr.techn. Georgi Shilyashki

durchgeführt am

Institute of Electrodynamics, Microwave and Circuit Engineering
Technische Universität Wien

Ivo Matković

Lerchenfelderstraße 19, 1070 Wien,
Matr. Nr. 9827175

Wien, im November 2016

Abstract

Magnetic cores of transformers, shunt reactors, electric motors, generators, rotating machines etc. exhibit very complex flux distributions. As it is well known, the variations of the local inductions, but also fluxes in normal and transverse direction tend to influence the core losses and the magnetostriction in a very significant way. For improvements and optimizations of the magnetic cores, aiming lower losses and audible noise, the evaluations of the local induction values are an inevitable task. Furthermore, the correct detection of the induction out of the rolling direction for assessment of the rotational magnetization is of a great significance for industry, in particular for transformer core manufacturers.

Established methods of local induction measurement, such as drilling holes in the laminations and inserting pick up coils, are extremely laborious as well as destructive for the cores. In the current work, a novel tangential induction sensor was manufactured and is presented. With this sensor, non-destructive measurements, not only on the surface, but also in core interior should be possible. Contrary to the traditional tangential H-sensors, the current sensor possess a very thin nanocrystalline ribbon as a "dummy" core. Around the ribbon a thin wire (≈ 50 μm) is wounded. Placed in a location of a laminated core with unknown induction B, the sensor is magnetized with Bs. In most likely case, both inductions deviate from each other, on one hand side due to the different permeabilities and on the other due to existing demagnetizing field. However, using a priori calibrated function $B(B\text{s})$, the unknown induction can be evaluated.

A very important part of the concept of the tangential induction sensor is the calibration of the sensor. The sensor can be calibrated in an Epstein frame, or in a region of laminated core of well-known induction. However, in the current work, measurements not only in the rolling direction, but also for two other important directions were performed for assessment of rotational magnetization. Therefore, an individual sensor was not sufficient. For that aim, in the current work, a set of sensors was used placed on a thin Kapton® foil, attached to the surface of a hexagonal grain oriented sample. The sensors were

placed in rolling direction, in transverse direction (TD) and in 30° angle to the RD. The calibration was performed by means of a Vienna Rotational Single Sheet Tester.

As shown in a previous work, the resolution of the nanocrystalline sensors depend strongly on the used geometry. For that purpose, three sensor sets with different lengths and widths of the nanocrystalline ribbons are prepared, tested and compared with each other. In an individual set, all three sensors are of the same dimensions. The longest set of sensors tend to be not useful at all, even for low induction values *B*. Due to the high length of the sensor, the demagnetizing effect tend to be very weak, and it reaches saturation for $B > 0.6$ T, due to the extremely high initial permeability values of the nanocrystalline material ($\mu_r \approx 100000$) . The sensor set of middle length exhibits excellent resolution for low induction values *B*, but is not effective for a magnetization above 1.1 T due to saturation effects. On the other side, the widest and shortest set of sensors tend to exhibit the best results, good resolution for high *B*, and sufficient resolution for low *B*.

The presented sets of sensors were tested in a 3-phase, 3-limb transformer core. The sensor shows good results of the measured induction for the rolling direction. However, it was not very effective for the transverse direction, mainly due to saturation effects. For the interpretation of the achieved results, numerical simulations are presented. They are performed by a novel MACC (Multi-directionally non-linear magnetic equivalent circuit calculation) method, developed by our group.

Contents

1. Introduction

Magnetic cores of transformers, shunt reactors, electric motors, generators, rotating machines etc. exhibit complex flux distributions. As it is well known, the variations of the local inductions B may cause strong increase of the losses P and magnetostriction λ, due to the non-linear dependences $\lambda(B)$ and $P(B)$. For example, an increase of the induction B by 1 % means increase of the losses P by ca. 2% [1]. Furthermore, normal fluxes (off-plane fluxes) distributed perpendicular to the plane of magnetization [2] may increase the magnetostriction in a distinct way, as it was shown in our own work for the case of grain oriented (GO) materials [3]. In particular, for grain oriented materials, deviations of the magnetic flux out of the rolling direction in form of rotational magnetization cause strong increases of losses and audible noise [4, 5], representing a significant problem of high practical relevance.

For improvements and optimizations of the magnetic cores, aiming lower losses and audible noise, the evaluations of the local induction values is an inevitable task. Established methods of local induction measurement, such as drilling holes in the laminations and inserting pick up coils [6, 7], are extremely laborious as well as destructive for the cores. Due to the mentioned reasons, the search coils are often wounded around the whole packages [8 - 10] or around some laminations. The later tend to impede the spatial resolution of the measurement in significant ways. Another approach for measurements of the induction is the needle method [11]. However, this method needs striping of the coating of the lamination and can be performed only on the surface of the material.

Recently, a series of novel sensors were designed and developed by our group. The basic concept of all the sensors is described in [12]. In [13], the pin sensor was presented. It represents an a priori calibrated pure iron pin, which is inserted in a specially prepared magnetizing channel. The sensor showed very good results for induction in rolling direction above 1.5 T. However, a significant disadvantage of the sensor is the preparation of the measurement channels. With that sensor, only measurements in rolling direction and for inductions $B > 1.5$ T are possible.

In [14, 15] the tangential induction sensor with a Si-Fe, used as a core is presented. Contrary to the traditional tangential H-coils, our *induction* sensor exhibit a nanocrystalline ribbon as a "dummy" core. Around the ribbon a thin wire (≈ 50 μm) is wounded. Placed in a location of a laminated core with unknown induction *B*, the sensor is magnetized with *B*s. In most likely case, both inductions deviate from each other, on one hand side due to the different permeabilities and on the other due to existing demagnetizing field. However, using apriori calibrated function *B*(*B*s), the unknown induction can be evaluated. However, tangential sensors with Si-Fe as a ribbon are suitable only for the core surface mainly due to the high thickness of the Si-Fe lamination. Such a sensor placed between the laminations of a magnetic core would cause a significant air gap and would influence the local flux distribution in a significant way.

The basic idea of the current work, presented firstly in [16] is to exchange the Si-Fe ribbon with a nanocrystalline one. The aim is to take advantage of the unique properties of the nanocrystaline material. Apart from its low thickness (about 20 μm), enabling measurements not only on the surface, but also in the core interior, it possess very high values of permeability ($\mu_r > 100\,000$) and relative high saturation magnetization ($B_S \approx 1.3$ T). Contrary to Fe-based amorphous materials of the same thickness, a further important advantage of the nanocrystalline ribbon is its non-sensitivity to mechanical stress, due to its almost zero magnetostriction.

As already mentioned, a very important part of the concept of the tangential induction sensor is the calibration of the sensor, presented. In our previous work [16], the sensor was calibrated in an Epstein frame, or in a region of laminated core of well-known induction. However, for the detection of the rotational magnetization, an individual sensor is not sufficient. Therefore, in the current work, a set of sensors was used placed on a thin kapton foil, attached to the surface of a hexagonal grain oriented sample. The sensors were placed in rolling direction, in transverse direction (TD) and in 30° angle to the RD. The calibration was performed by means of our Rotational Single Sheet Tester.

As shown in a previous work, the resolution of the nanocrystalline sensors depend strongly on the used geometry. Sensors of high length tend to have

excellent resolution for low nominal induction values B_{NOM}, but they are not effective for high magnetizations due to saturation effects. On the other side, sensors of short length tend to exhibit good resolution for high B_{NOM}, but are not suitable for low B_{NOM}, due to strong demagnetizing effects. The latter show that an optimization of the sensor geometry was of significant importance. Therefore, three different sets of sensors with different geometries were manufactured calibrated and tested.

2 Magnetic Induction Sensors

All novel sensors which are presented in this chapter have one thing in common: they first need to be calibrated in order to be used for actual measurement of magnetic induction. Process of calibration is described in detail in the next chapter.

Before describing novel sensors to measure local values of magnetic induction, it is important to mention the two most common methods of determining *B* for a laminated transformer core.

2.1 Traditional Methods

2.1.1 Search Coil Method

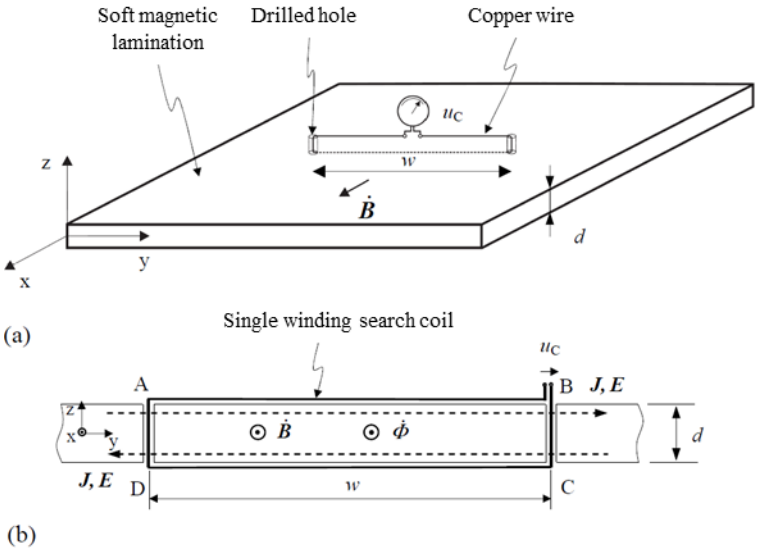

Figure 1 Search coil Method. a) View of the surface of the sample. b) Cross-section view. From [20]

Schematic outline of the search coil method can be seen in Figure 1. Two holes are drilled in the lamination and single winding of thin copper wire is put through. With known area of the cross-section encompassed by the wire, and measuring the induced voltage signal $u_C(t)$ at the ends of the wire, B is calculated by integration over time. The corresponding equation being:

$$B_X = -\frac{\int_0^T u_C(t)dt}{wd}$$

Biggest disadvantages of using this method are: 1) that it is extremely laborious, as drilling of laminations is necessary, 2) holes damage the structure of the material, and 3) wires leave air gaps between the laminations.

2.1.2 Needle Method

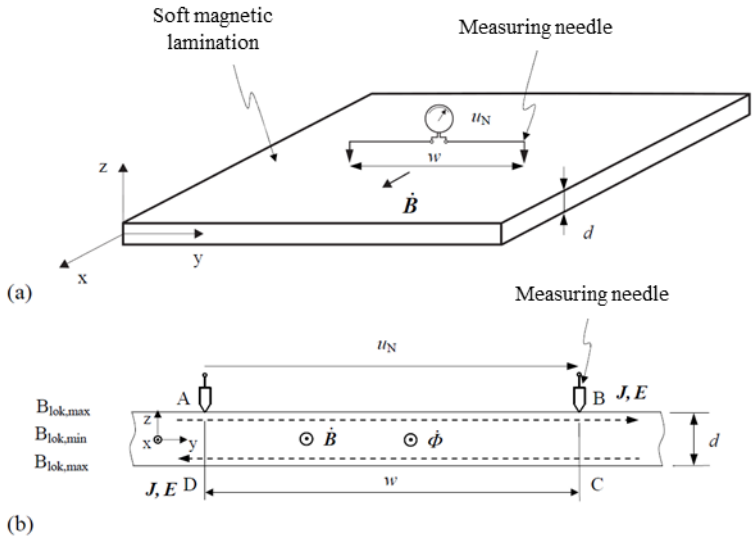

Figure 2 Needle Method. a) View of the surface of the sample. b) Cross-section view. From [20]

Underlying principle of the Needle Method is shown in Figure 2. Instead of drilling holes, the insulating coating is removed in a spot like way and two needle contacts are pressed on to blank spots A and B. Magnetic induction *B* can then be calculated using the equation:

$$B_X = -\frac{2\int_0^T u_N(t)dt}{wd}$$

The detected voltage $u_N(t)$ reflects 50% of the corresponding voltage $u_C(t)$, provided that symmetric conditions are given.

Again, this method has some considerable limitations: 1) removing insulation is laborious, and 2) it is possible to determine magnetic induction only on the surface of the laminated core. Measurements inside the core are not achievable.

2.2 Pin Sensor

First kind of novel sensors we present is the pin sensor.

Pin sensor technique is a novel method to determine 3-dimensional distribution of magnetic induction. It utilizes the fact that some transformer cores possess vertical holes due to the manufacturing process. These holes can be used as "measuring channels" to determine the flux distribution along different heights inside the transformer core. Even if the core does not have enough vertical holes, several other holes can easily be drilled in order to get a more complete picture of 3-d flux distribution. Although drilling holes through the laminations of a transformer core is arduous, it is not as burdensome as the conventional method of using single-turn search coils: it does not involve as much drilling, and, even more important, it avoids the use of wires, which cause inevitable air gaps.

The basic idea is to insert an iron rod, called "pin", of slightly smaller radius than the existing hole, which has a built in search coil. This search coil "picks up" some value of the local magnetic induction, which in turn induces a voltage signal. Pin sensor is placed in a spot where *B* is well-known (such as middle of the outer limb) and can be varied. The induced voltage signal *u* is then measured for various values of *B*, and later "translated" into the local induction

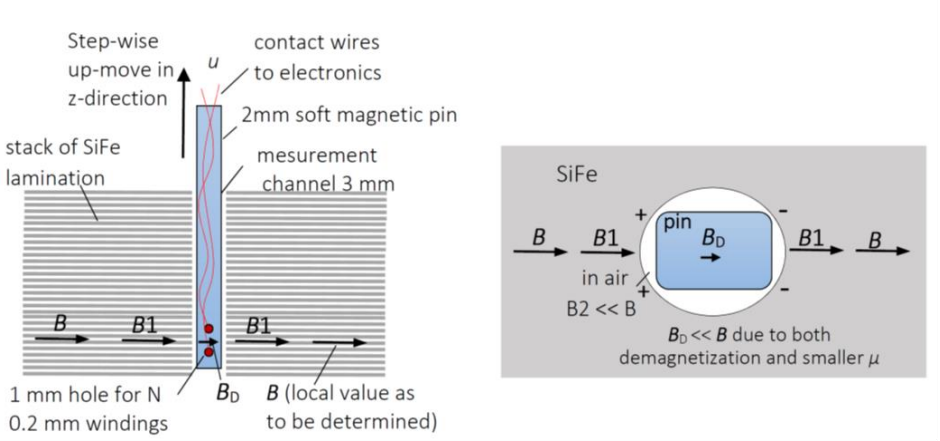

Figure 3 Pin sensor technique for induction measurements in the interior of a soft magnetic system like a machine core. (a) thin measurement channel is drilled through the system, and a pin is inserted that carries a search coil at its soft magnetic end region. (b) View from above. From [12]

value B_1 by means of transfer function (calibration function) stored in a computer file. This function can they be used to determine *B* at other drilled holes of the transformer core, at various heights. For more, see [12].

It is to be noted that a calibration function is only valid for one diameter of the hole. For each hole diameter, a new calibration curve has to be recorded.

2.3 Tangential Induction Sensor

Single sheet testers (SST), which have become a standard alternative to the Epstein frame for testing of electrical steel use tangential field coils to determine magnetic field intensity *H*, inside the magnetic material. A field coil with a very high number of turns is placed along the surface of the magnetic material. Basic principle of a tangential field coil is shown in Figure 4.

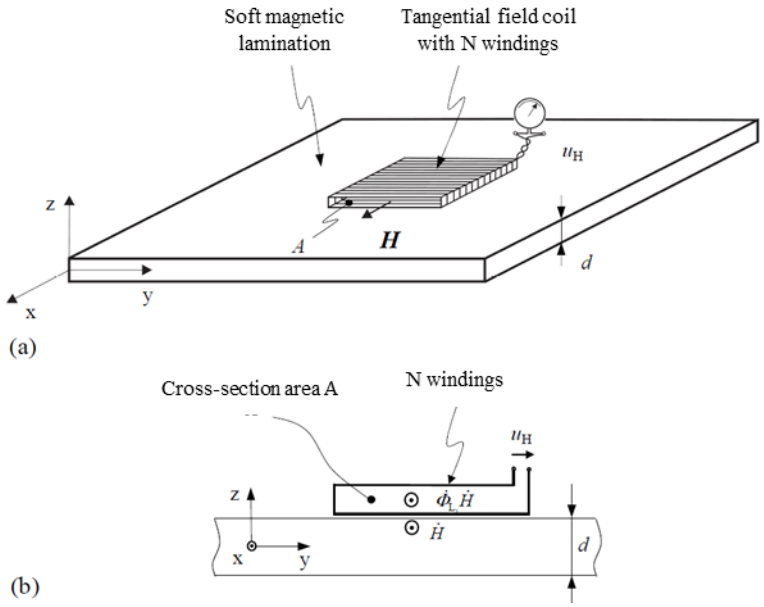

Figure 4 Tangential field coil. From [20]

Due to the continuity condition, the tangential component of magnetic field intensity H_t through the coil is the same as inside the material. By integrating the voltage u_H measured at the ends of the field coil over time, we can determine the unknown value of H_t inside the magnetic material. The corresponding equation is given below, where *N* is the number of turns and *A* the cross section of the tangential coil.

$$H_t = -\frac{\int_0^T u_H(t)dt}{\mu_0 NA}$$

Tangential induction sensors operate on the same principle. The sensor is made out of the same ferromagnetic material as the transformer core, around which thin copper wire is wound. According to the continuity condition described above, the tangential components of magnetic field strength in the sensor and on the surface of the core have to be the same. However, due to the several factors, such as the air gap between the core and the ferromagnetic sensor due to the wire, and the demagnetizing field, these values are not the same.
Therefore, as in Pin sensor measurements, a calibration has to be carried out. A part of the transformer core with a well-defined magnetic induction (such as

the middle-, or the outer limb) is chosen, and the calibration curve is recorded. It can then be used as a transfer function for measurements of other parts of the core.

This is a non-invasive method of measurement of local magnetic induction. Therefore, only measurements at the surface of the core are possible. Still, in combination with the Pin method, a fairly complete picture of the 3D distribution of the magnetic flux for the entire core can be obtained.

Figure 5 An example of a tangential induction sensor for the non-invasive measurement induction of the induction B(t) at the surface region of a transformer core.

2.4 Amorphous Alloy Sensor

Amorphous alloys with soft magnetic properties are made from 70 to 80% Fe, Ni, Co metal atoms, and 20 to 30% of B, C or Si which are metalloid glasses. Crucial step the production of amorphous alloys is rapid cooling of the material which is in liquid state. Cooling rates of 10^5 to 10^6 K/s are needed. As the material solidifies, crystalline arrangement of atoms is effectively destroyed, and the atomic structure resembles that of a melt [19]. The result is usually a ribbon with a thickness of around 20 µm to 30 µm.

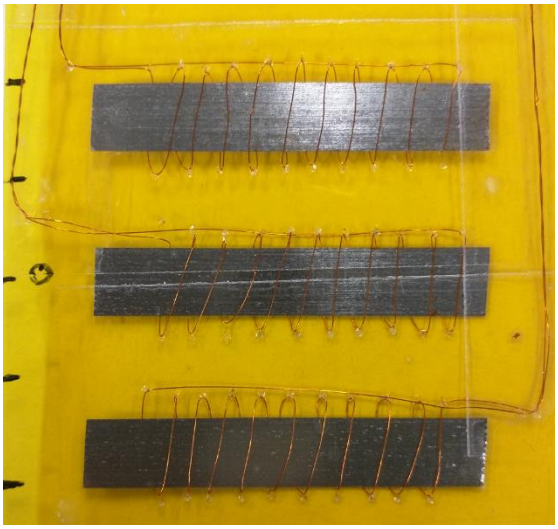

Figure 6 Tangential induction sensors using an amorphous alloy ribbon as a core, with few windings of 100µm thin wire as a pick-up coil.

In the scope of this thesis, one such ribbon was used to manufacture a sensor which can be seen in Figure 6. As can be seen, this sensor can simultaneously measure flux in rolling direction at three different points. Major advantage is that this sensor can be placed between the laminations, inside the transformer core.

The length of each ribbon was around 50 mm with a width of about 10 mm. In addition, copper wire with a diameter of 50 µm was used. Each ribbon has 10 windings around it in order to achieve good resolution even at smaller values of magnetic induction. Completed sensor was still flat enough (maximum of 150 µm including Kapton® foil) to place between the laminations without causing major air gaps.

Here again, calibration was needed to record all possible values of magnetic induction in the transformer core *B*, as a function of magnetic induction detected by the sensor B_S.

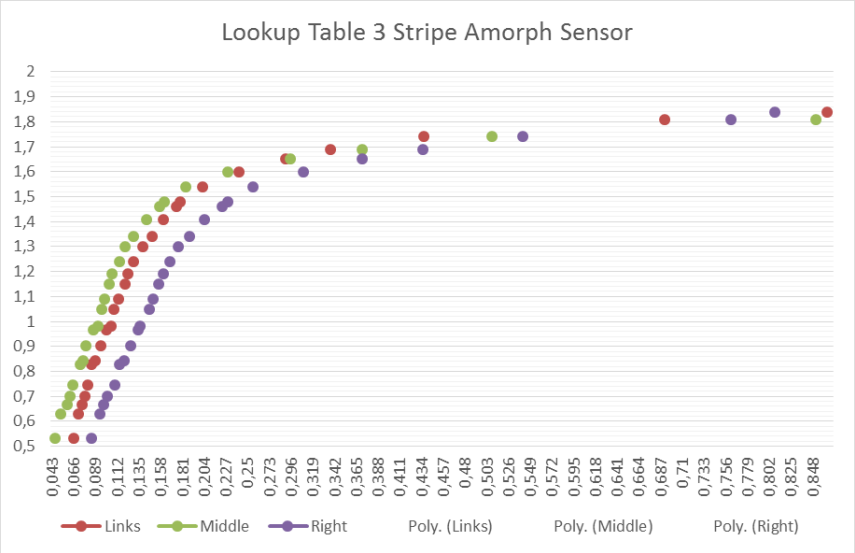

Figure 7 Three calibration curves of the three-stripe amorphous ribbon sensor according to Fig 5.

For the purpose of this thesis, calibration was performed inside two specific transformer cores. Both were three-limb transformers with near circular cross-section of each limb. Meaning they had lamination packages of different width. Sensor was put in the middle package of one of the outer limbs of the transformer. The induction in the core was monitored with a control coil around the outer limb. For each core a separate calibration process is required. Apart from the obvious cases when there is a difference in core material, or core geometry, even nominally same transformers can exhibit differences because of anisotropy, hysteresis and differences that occur during the manufacturing process. A calibration curve for one of the examined transformer cores can be seen in Figure 7.

Ona major disadvantage of amorphous magnetic materials is their sensitivity to mechanical stress. Laminations of a modern transformer core are kept together by clamping. A sensor made of amorphous material changes its properties when placed between the laminations of a transformer core, which is then clamped together. Clamping needs to be tight in order to avoid air gaps which might occur. Measurements of the two cores were very difficult, since for each measurement the clamping had to be removed in order to place the sensor in a desired position.

2.5 Nanocrystalline Sensor

Nanocrystalline alloys are very similar to amorphous alloys both in chemical composition and in production process. In fact nanocrystalline materials are produced out of an amorphous alloy which is heated and then subjected to a process called rapid solidification technology [16]. This involves cooling the alloy at an extremely high rate which leads to forming of fine grain structure. Size of these fine grains is around 10 to 15 nm. In order to produce a nanocrystalline material, *Cu* and *Nb* are added to a *FeSi* based alloy. Copper and Niobium are responsible for enhancing and inhibiting the formation of nanocrystallites, which are made of arrays of Fe3Si nanoparticles, and are surrounded by amorphous matter [19].

Such materials exhibit very favorable physical properties, such as low thickness (about 20 μm), high electrical resistance of about 1,1 μΩm, and they are not susceptible to mechanical strain.

Low thickness is important because such a sensor can be placed between the laminations to perform measurements **inside the core**. Air gaps are still unavoidable, but can be reduced to a somewhat acceptable degree. This means no drilling, or other actions destructive for the core are necessary. Also, since the material is immune to mechanical strain, nanocrystalline sensor is not affected by clamping. Clamping is necessary to keep the sheets of a transformer core together. This is one major advantage of the nanocrystalline materials compared to amorphous alloys.

Magnetic properties of nanocrystalline alloys are also very favorable: high values of permeability ($\mu_r > 100\,000$), relative high saturation magnetization ($B_S \approx 1.3$ T); and minimal magnetostriction, since as mentioned above, it keep its magnetic characteristics even under mechanical stress.

First attempts to build a magnetic induction sensor with a nanocrystalline material for this thesis were driven with the goal to achieve absolutely minimal sensor height. This would ensure minimal air gaps between the laminations when a sensor was inserted at a particular point inside the transformer core. In

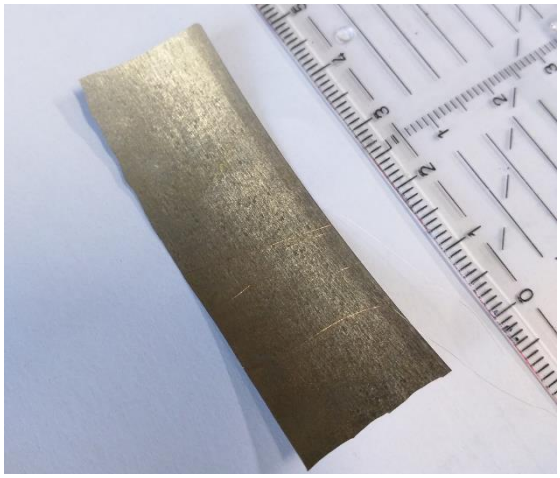

Figure 8 One of the first versions of a nanocrystalline sensor. It involved a nanocrystalline strip of 20µm thickness. A pick-up coil of 25µm copper wire can hardly be seen. Basic problems result from difficulties to cut the ribbon.

order to accomplish this, it was tried to wind a copper wire of just 25µm in diameter around just one loose nanocrystalline strip. No Kapton® foil was used. Dimensions of the strip were roughly 50 mm x 15 mm. Copper wire was wound 6 times around the strip. This way the entire sensor had a height of maximum 80 um. In can even be argued that this sensor even had a height of around 50 um, since the windings on the each side of the strip (over and under) were not directly on top of each other. This simple sensor can be seen in Figure 8.

For this first effort with nanocrystalline ribbons, calibration was performed in the transformer core, specifically inside the middle of the outer limb, where alternating magnetic induction was assumed. This assumption holds true in basically all modern transformer cores. After the calibration curve has been recorded, sensor was placed in different parts of the transformer core, and magnetic induction was measured. This sensor has obvious drawbacks and limitations. First of all, it is extremely hard to handle, because nanocrystalline is brittle and can break at any time when it is being held. Second, the copper wire of such a small diameter is light and snaps if it experiences any kind of pulling. Additionally, such thin wire is easily damaged when attempting to remove the isolation coating.

2.6 3-D Nanocrystalline Sensor

All the aforementioned sensors have one thing in common: they can deliver values of local flux distributions only in **one direction**. As has been mentioned before, flux distributions in a transformer core are very complex and also significant, since they are responsible for losses and audible noise. Therefore, a novel sensor based on the nanocrystalline sensor was proposed, to try to measure flux in **three directions** simultaneously. If successful, this could give us some idea about the **rotational magnetization** (RM), which is typical for some areas of the transformer core. Rotational magnetization appears when the vector of magnetic induction *B* diverges from the preferred rolling direction during the magnetization cycle. RM brings about considerable increase in losses. Therefore, it is important to study it and develop ways to reduce it.

3 Measurement and results

3.1 Rotational Single Sheet Tester

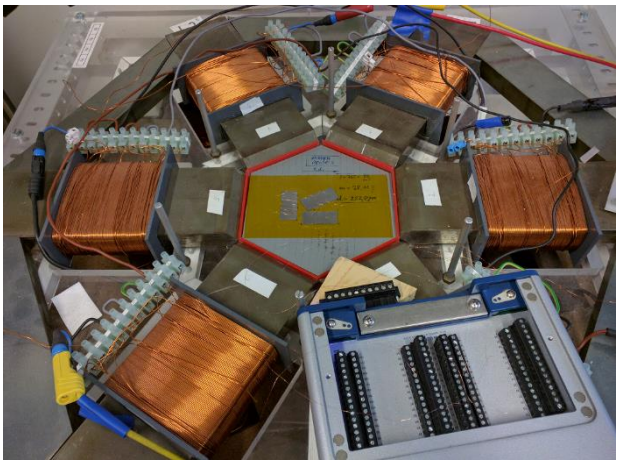

Figure 9 Rotational Single Sheet Tester as used for the calibration and testing of the nanocrystalline sensors.

In order to calibrate the nanocrystalline sensors for this thesis, the Vienna Rotational Single Sheet Tester (RSST) which was developed at Technology University of Vienna, at the Institute of Electrodynamics, Microwave and

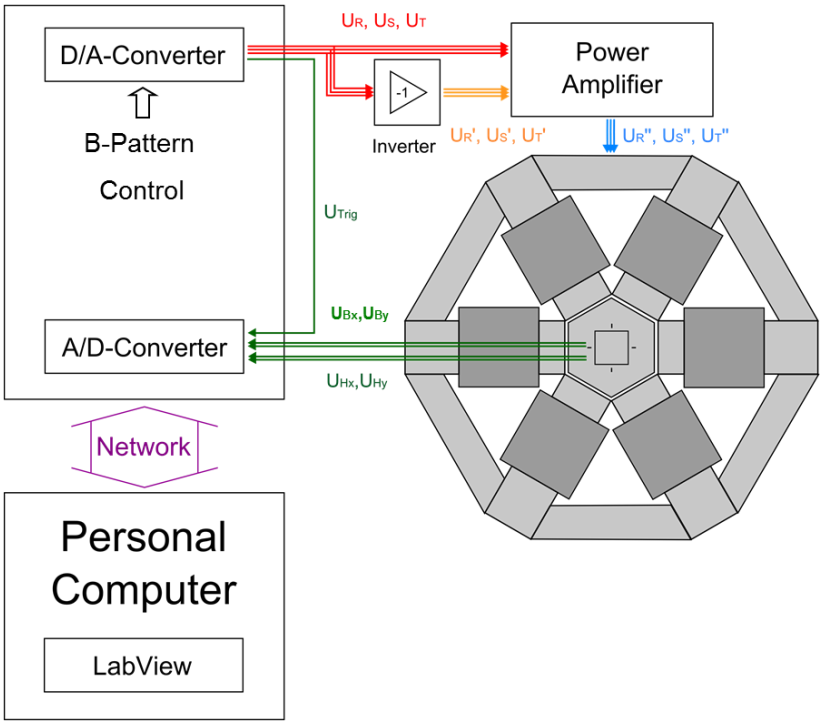

Figure 10 Basic structure and mode of operation of the RSST. See [17]

Circuit Engineering was used. Most important parts of RSST and its functionality can be seen in Figure 10.

Central part of the RSST is reserved for a single, hexagonally cut lamination sample ("single sheet").

Due to the distinctive anisotropy of modern transformer materials, great care needs to be taken when cutting the sample. The rolling direction of the sample has to match the rolling direction of the RSST.

Hexagonal sheet is surrounded by six laminated iron cores, assembled at a 60° angle to each other, so that they form a hexagonal structure that correlates to the investigated sample. Each of the six cores has 340 windings of copper wire around it. By controlling the current through the wires, the flux in the cores is regulated. They are paired together in such a way (U_R' with U_R'', and so forth) that only three control variables are needed. Pattern control is handled by a LabView® program. Before the control voltages reach the RSST, they pass

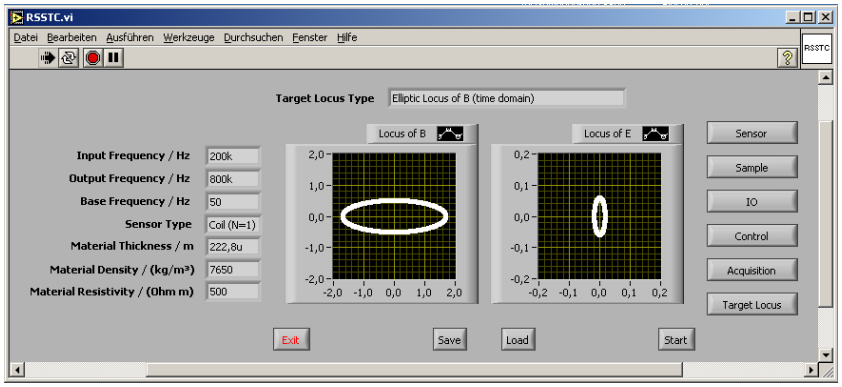

Figure 11 Snapshot of the control part of Lab View program for RSST

through a power amplifier.

Figure 11 shows a control panel of the LabView® program where all necessary data about the sample hast to be inserted. This data includes dimensions of the sample (most importantly its thickness), material density given in kg/m^3, specific material resistivity in Ω/m, and so on. Furthermore, the values of induction in the rolling direction B_{RD} and aspect ratio a are set. These values shall be explained later. Lastly, a pattern of magnetic flux density is to be chosen. Rotational magnetization usually has elliptical, or rhombic form. Both of these can be generated by the RSST.

Part of the RSST which measures the magnetic flux in the sample induced by surrounding iron cores is twofold, using both the needle method to acquire values of magnetic flux density in rolling and transverse directions (marked by B_X and B_y), and the tangential induction method to get the corresponding magnetic field values (H_X and H_Y). The four needles and the two tangential inductors can be found in the center part of where the sample is placed, so that they are directly underneath and have contact.

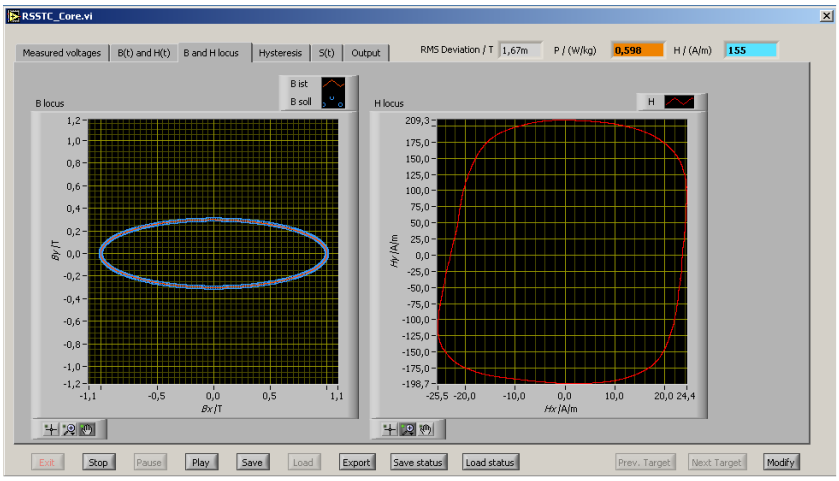

Figure 12 Example of a magnetic pattern attained in the sample, With locus of B and H shown

These variables measured directly in the sample are then transferred back to the RSST via its own feedback control system. Measured values of B_X and B_Y are compared to the desired values constantly, and the exciter currents in the windings are adjusted until chosen values of B_X and B_Y are achieved with sufficient accuracy.

An example of resulting loci of B and H, can be seen in Figure 12. Left part shows locus the magnetic induction for B_X = 1T and a = 0,3. Blue ellipse shows the desired B locus, while the thinner, while red ellipse the reached locus. Right part shows the locus of H. It shows value of H_Y which is ten times bigger than the H_X. When the aspect ratio of 0,3 is taken into account, it the multiplying factor raises to 30. This considerably high value of H_Y is the **main reason for saturation** in TD and 30° directions. Saturation is discussed in the results below.

For the purpose of this thesis, sheets of highly grain-oriented material 23ZDKH90 have been used. Properties of 23ZDKH90 are given in the table below. Testing with other types of electrical steel are possible, but would exceed the scope of this thesis. Results of RSST measurements were verified on a model transformer built with the same material.

Table 1 Catalogue data of the 27ZDKH90 electrical steel.

Thickness	Density	Resistivity	Core Loss	Induction
0,27mm	7650 kg/cm^3	0,5μΩm	0,9 W/kg	1,9T

3.2 Calibration

Process of sensor calibration can for our purposes be explained in the following way:

A sensor is placed in a particular setting, which is similar to the environment of the desired object to be investigated (measured). More specifically, sensor is placed in a setting with well defined, changeable and controllable magnetic induction B. Then, the strength of magnetic induction in this environment B_{NOM} is varied in a desired interval (usually form 0T to 1,8T) with a desired resolution. During this process, the strength of magnetic induction in the sensor B_S is recorded. Detected induction B_S is generally different from environment induction B_{NOM}, and it is also of a much smaller value, due to inevitable air gaps, demagnetizing fields, and so forth. Once the entire range of B_{NOM} has been passed through, an empirical function $B_S(B_{NOM})$ is generated. The inverse function of this empirical function, namely $B_{NOM}(B_S)$, is now a powerful tool which can be used (together with, of course, our sensor) to measure B_{NOM} in other similar environments. Sometimes the physical variable which is detected by the sensor is not even magnetic induction, but another one. Nevertheless, this other variable has to have a definite relation to B_{NOM}. For example, nanocrystalline sensors that were built actually detect the induced voltage u at the ends of the copper wire wound around the nanocrystalline strip. The time integral over the area of the cross-section of the strip then gives us the desired value of B_S.

3.3 Sensor Data

As was mentioned earlier, three different sensor geometries were produced.

First one with nanocrystalline ribbons of 15mm width, and the length of 30mm. This sensor also has the lowest number of windings, 8. Number of windings has been kept the same in all three directions.

Second sensor has nanocrystalline ribbons with the width of 10mm and length of 45mm, with 12 winding in all directions.

Third sensor has the smallest width of nanocrystalline material, which is 5mm, and length of 60mm. Number of windings increased to 16.

Measurements needed to attain the calibration curves were done by using the RSST, which was described earlier. Each sensor was placed on the top of the hexagonal single sheet lamination. The sample sheet was made out of the same

material as the model transformer core (23ZDKH90), which was essential in order to compare the results.

For each sensor, alternating magnetization was measured first. It consists of just the *B* component in the rolling direction, and no components in the TD or the 30 degree directions. Measurements between 0,1T and 1,85T were made, in 0,05T steps.

After that, the TD component of magnetic flux density was added. In this way rotational magnetization was introduced to the hexagonal sheet. Elliptical form of RM was chosen, although rhombic and skewed rhombic forms are also available. All three sensors were measured in presence of RM of different "strength". TD component of *B* was given as a ratio or the RD component.

$$a = \frac{B_{TD}}{B_{RD}}$$

The most common aspect ratios that can be observed inside specific regions of a transformer core of were measured. Those are 0,1 ; 0,2 and 0,3.

Results of all these measurements are given in the form of $B_S(B_{NOM}, a)$, and are presented in the next chapter.

3.4 Results

3.4.1 Sensor with wide and short Nanocrystalline Stripes

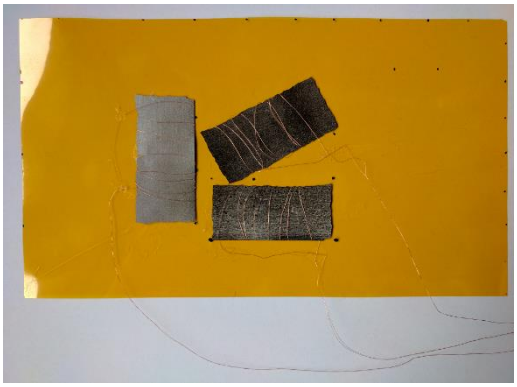

Figure 13 "Wide" sensor with three nanocrystalline ribbons of 15mm width and 30mm length.

This sensor has the biggest width of the three considered geometries. It had the overall best performance.

The calibration curve for the rolling direction exhibits a near linear dependency to the nominal magnetic induction B_{NOM}. This made for a sufficient resolution of the RD component for the entire measurement range [0,1T to 1,8T]. No signs of saturation could be seen, which makes it very useful for the measurements.

Even for the bigger aspect ratios between the TD and RD components of magnetic induction, the stripe placed in RD direction showed little signs of saturation.

The stripe in TD direction however, showed signs of saturation as soon as the TD component of B was introduced. Nevertheless, I found that values of B_{NOM} of up to 1,4T can be reliably measured for the aspect ratio of 0,1. For the aspect ratio of 0,2 one can also measure B_{NOM} up to 1,4T whereas at the aspect ratio of 0,3 only B_{NOM} values of up to 1T can be measured.

Stripe in the 30 degree angle also showed saturation as soon as the TD component was introduced. On average, the TD stripe provided better results for detection of rotational magnetization.

a = 0

RD ribbon shows excellent resolution over the entire range, which was surprising. I expected some signs of saturation above 1,3 T because of the material properties of nanocrystalline alloys.

TD and 30 degree directions also show good resolution. Although they are not applicable to the $a = 0$ case, they can still be used as a further proof of alternating magnetic induction, since their progression differs from the RM cases seen below.

a = 0,1

Again excellent characteristics of RD direction.

As expected, TD and 30 degree directions show saturation. TD can be used for B values up to 1,3T which is common for nanocrystalline ribbons.

Direction of 30 degrees shows saturation from as low as 0,4T. However, since TD produced applicable progression, RD can still be reliably predicted.

a=0,2

More of useful RD calibration, however uncertain data in TD direction, and saturation in 30 degrees make this doubtful for use.

a=0,3

Here RD direction shows some signs of saturation between 0,8T and 1,2T but shows good resolution for the values above. These questionable results are in any event not usable, since the TD direction shows noise effects and does not yield definite results.

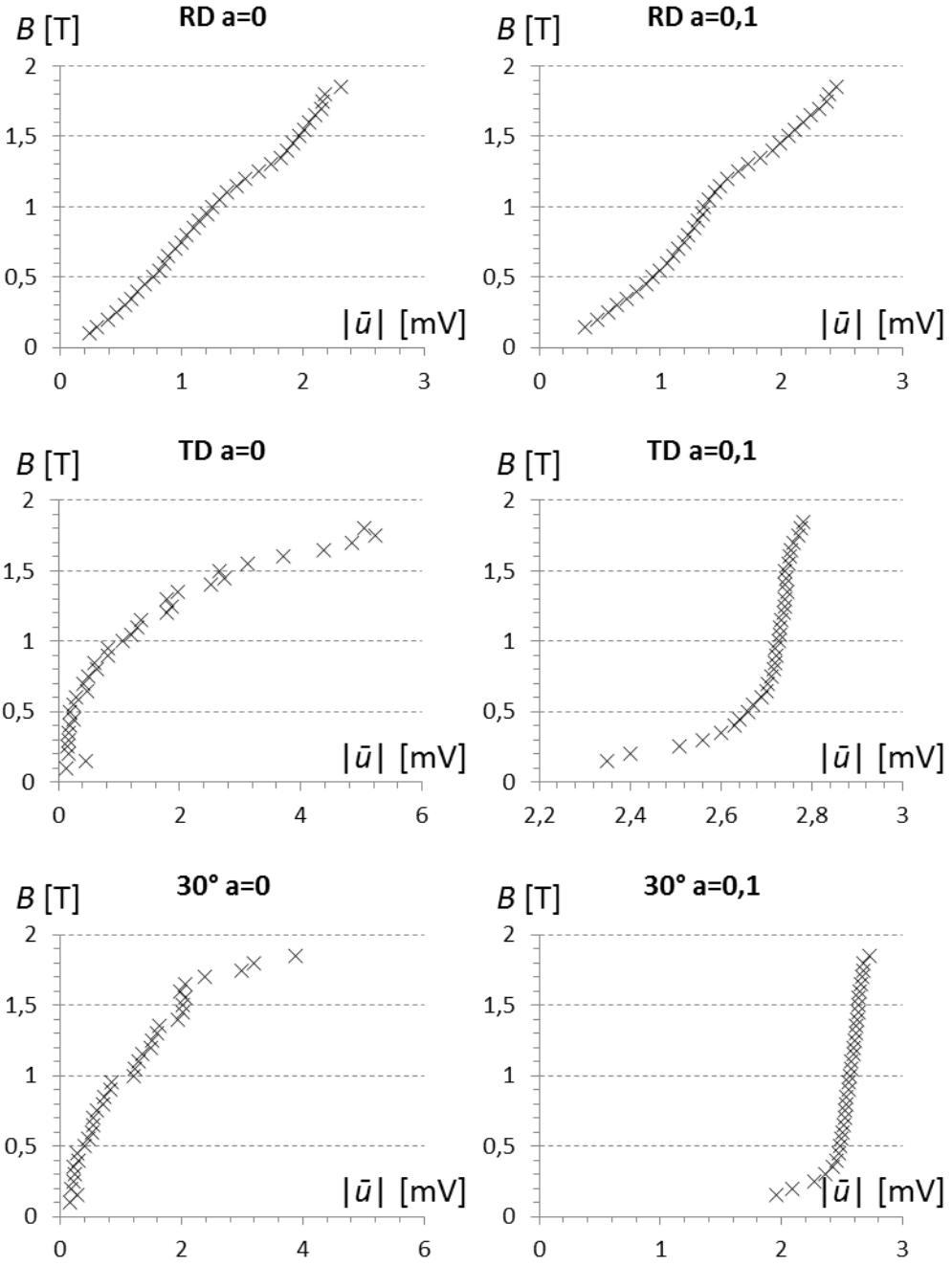

Figure 14 Examples of transfer curves for a nanocrystalline sensor of high width. The nominal induction value B (in T) is given as a function of the induced voltage u (in mV) in the windings of each strip. Case for a=0 is on the left side, case for a=0,1 on the right.

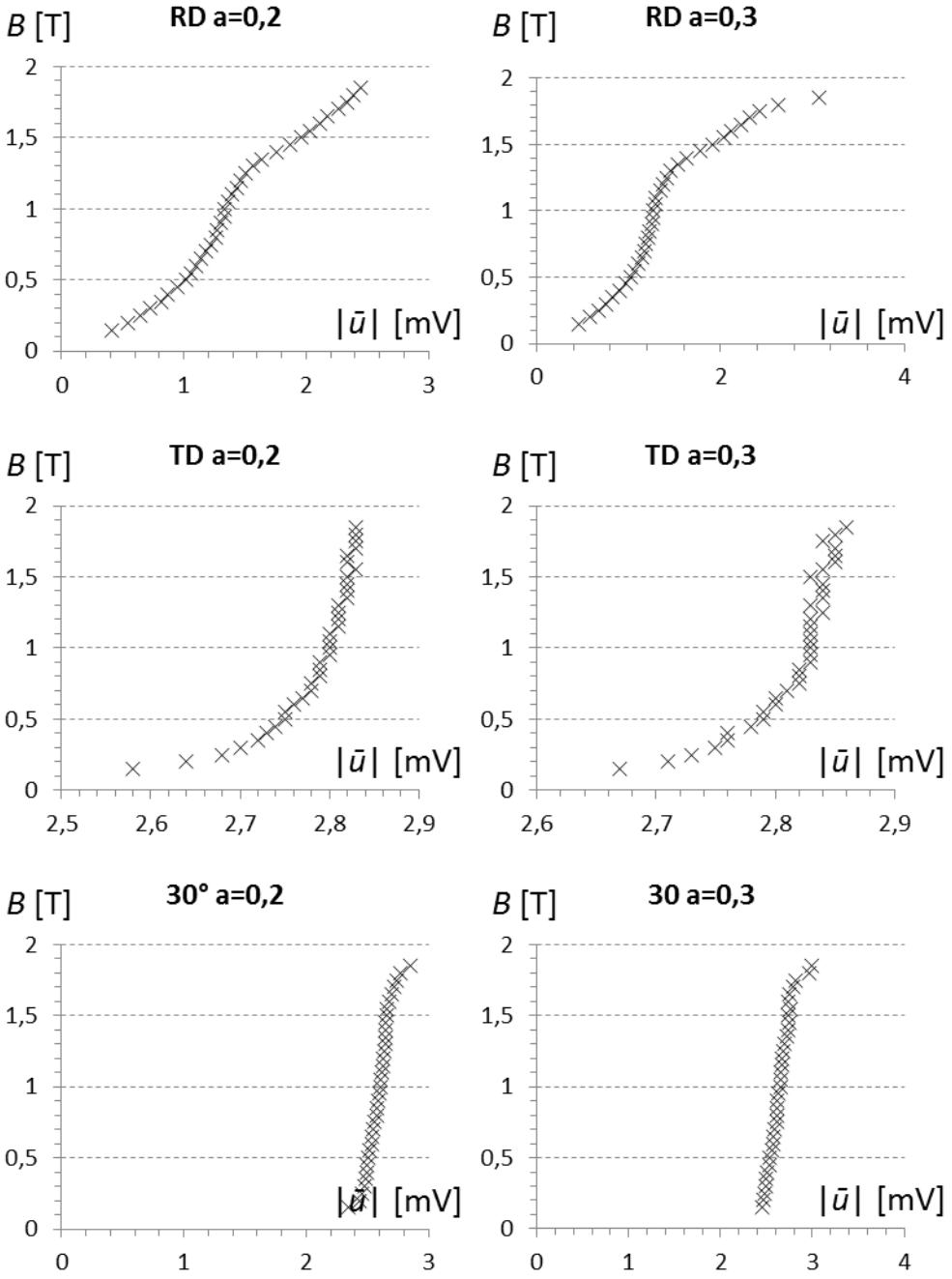

Figure 15 Examples of transfer curves for a nanocrystalline sensor of high width. The nominal induction value B (in T) is given as a function of the induced voltage u (in mV) in the windings of each strip. Case for a=0,2 is on the left side, case for a=0,3 on the right.

3.4.2 Sensor with middle Width and Length of Stripes

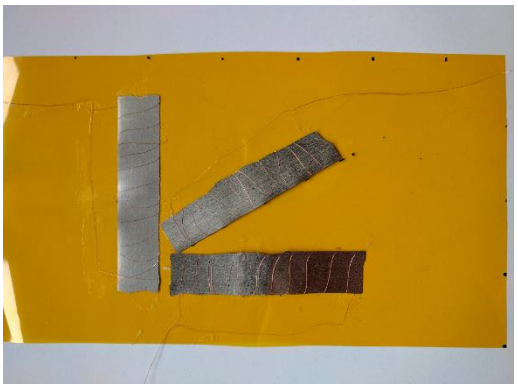

Figure 16 Sensor of "middle" width: three nanocrystalline ribbons of 10mm width and 50mm length.

This sensor has a middle value of width of the three considered geometries.

Had overall good performance, though not as good as the 15mm sensor.

The calibration curve for the rolling direction exhibits a near linear dependency to the nominal magnetic induction B_{NOM}. This made for a sufficient resolution of the RD component, but not for the entire measurement range. I found that values of B from 0,1T up to 1,5T could be reliably measured. Above 1,5T signs of saturation are clearly visible.

This behavior is visible for all values of the aspect ratio a.

However, the stripes in TD and 30 degree direction showed signs of saturation. They can nevertheless be useful as a confirmation of the presence of rotational magnetization, since transfer functions for RM case greatly differ from the alternating magnetization case ($a = 0$).

Also, some curves exhibited a disturbing jump at 1,1T for reasons that are not clear at this time.

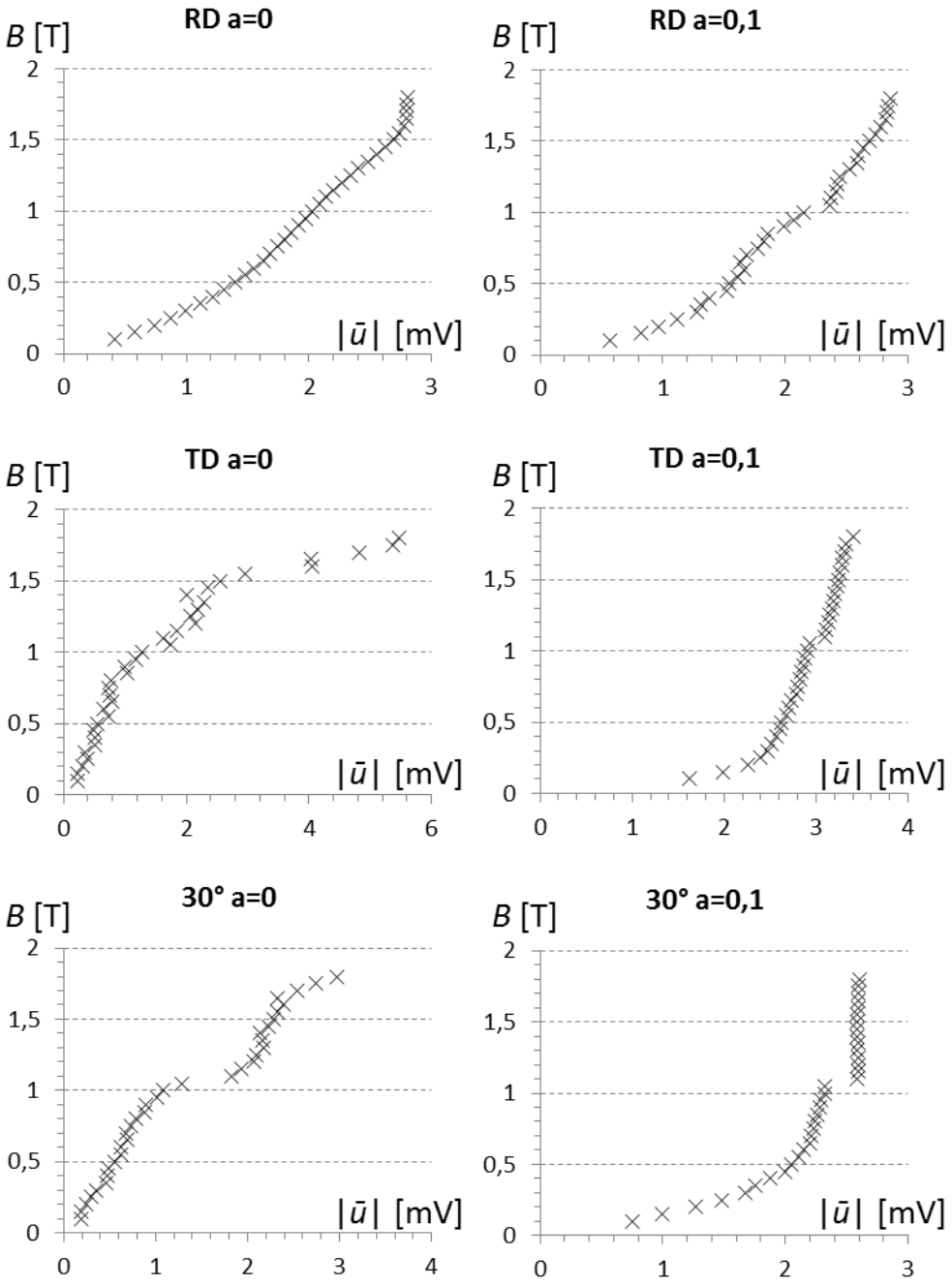

Figure 17 Examples of transfer curves for a nanocrystalline sensor of middle width. The nominal induction value B (in T) is given as a function of the induced voltage u (in mV) in the windings of each strip. Case for a=0 is on the left side, case for a=0,1 on the right.

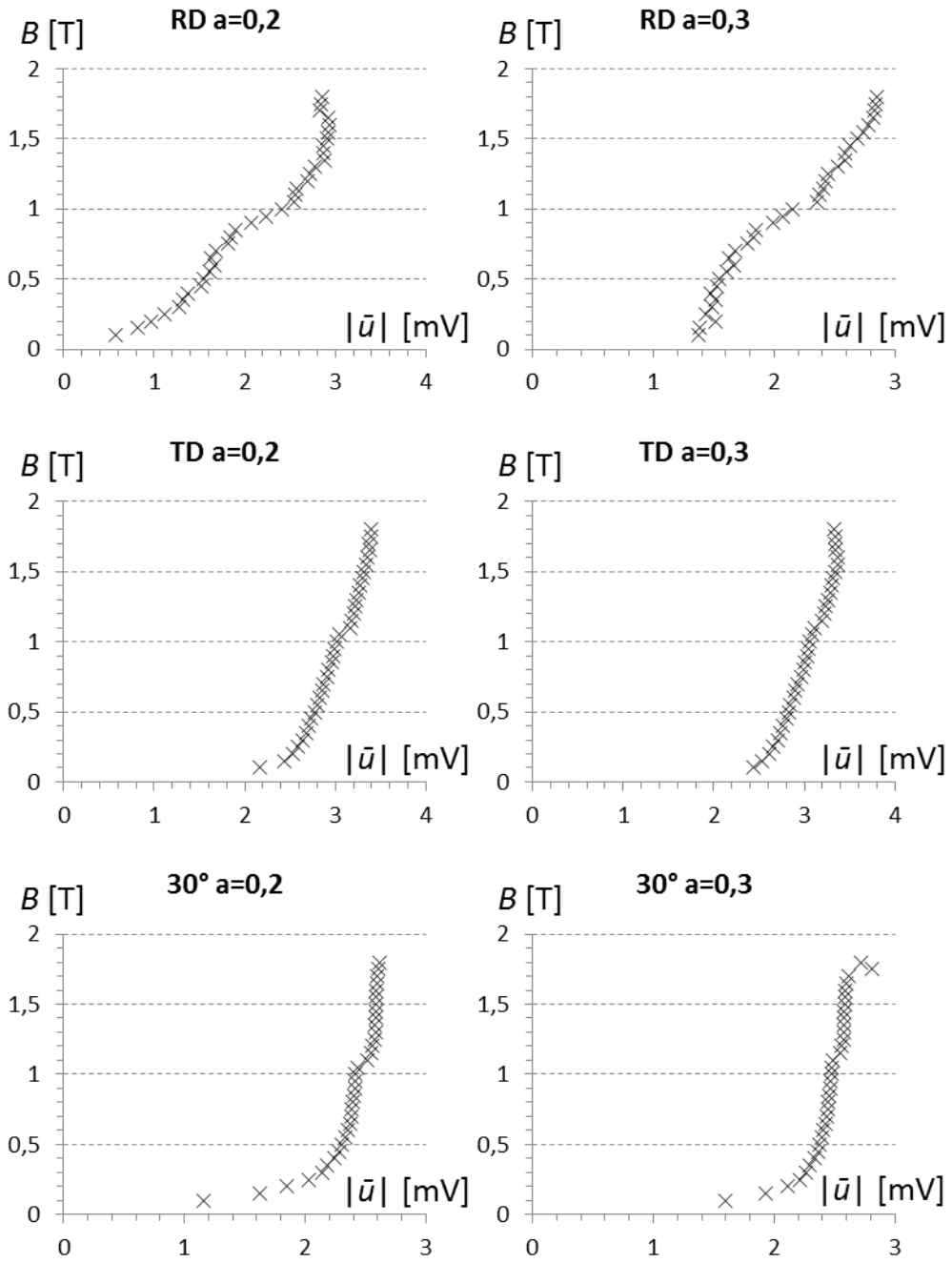

Figure 18 Examples of transfer curves for a nanocrystalline sensor of middle width. The nominal induction value B (in T) is given as a function of the induced voltage u (in mV) in the windings of each strip. Case for a=0,2 is on the left side, case for a=0,3 on the right.

3.4.3 Sensor with Ribbons of narrow Width and greater Length

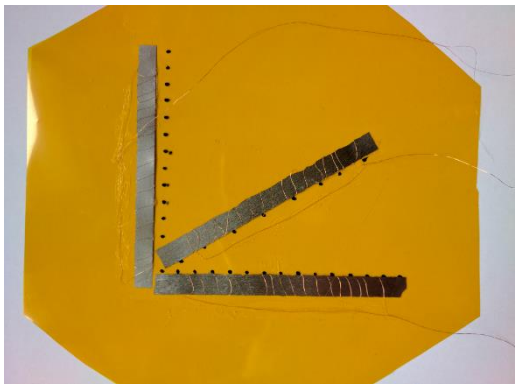

This sensor has the smallest width of the three considered geometries. It had the overall worst performance.

Saturation became apparent a low induction values.

With this sensor geometry, an even bigger problem started showing: measured values became instable. There was no clear and visible tendency, but rather an element of probability: disturbing jumps in the detected values, which makes the measurements with this geometry unreliable.

a = 0

The calibration curve for the rolling direction exhibits saturation for values of B_{NOM} above 0,5T. This made for a sufficient resolution of the RD component for the measurement up to 0,5T. RD shows signs of saturation above 0,5 T, which was not encountered with other two sensors. Even worse, it also shows instability. TD and 30 degrees show surprising resolution and stability. However, paired with unacceptable RD curve, they are of small value.

a = 0,1 – 0,3

Rather extreme instability in all three directions. Some patterns similar to previous curves are visible. Nevertheless, this level of noise makes the charts unusable.

This sensor had overall worst performance. Calibration curves had no sufficient accuracy for it to be used in further measurements. At this time I decided not to use this geometry either for verification on a model transformer core, or to perform a simulation.

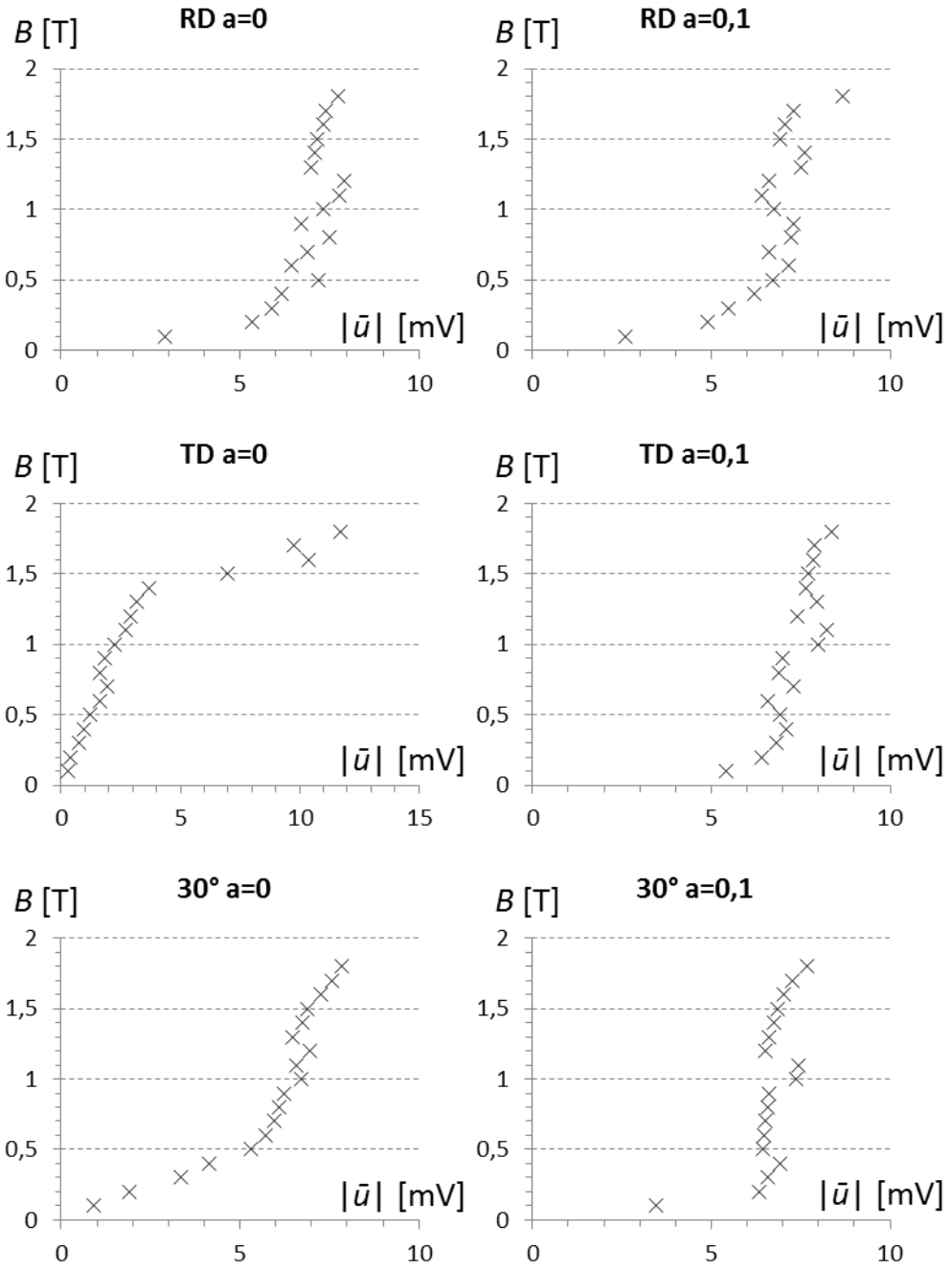

Figure 19 Examples of transfer curves for a nanocrystalline sensor of small width. The nominal induction value B (in T) is given as a function of the induced voltage u (in mV) in the windings of each strip. Case for a=0 is on the left side, case for a=0,1 on the right.

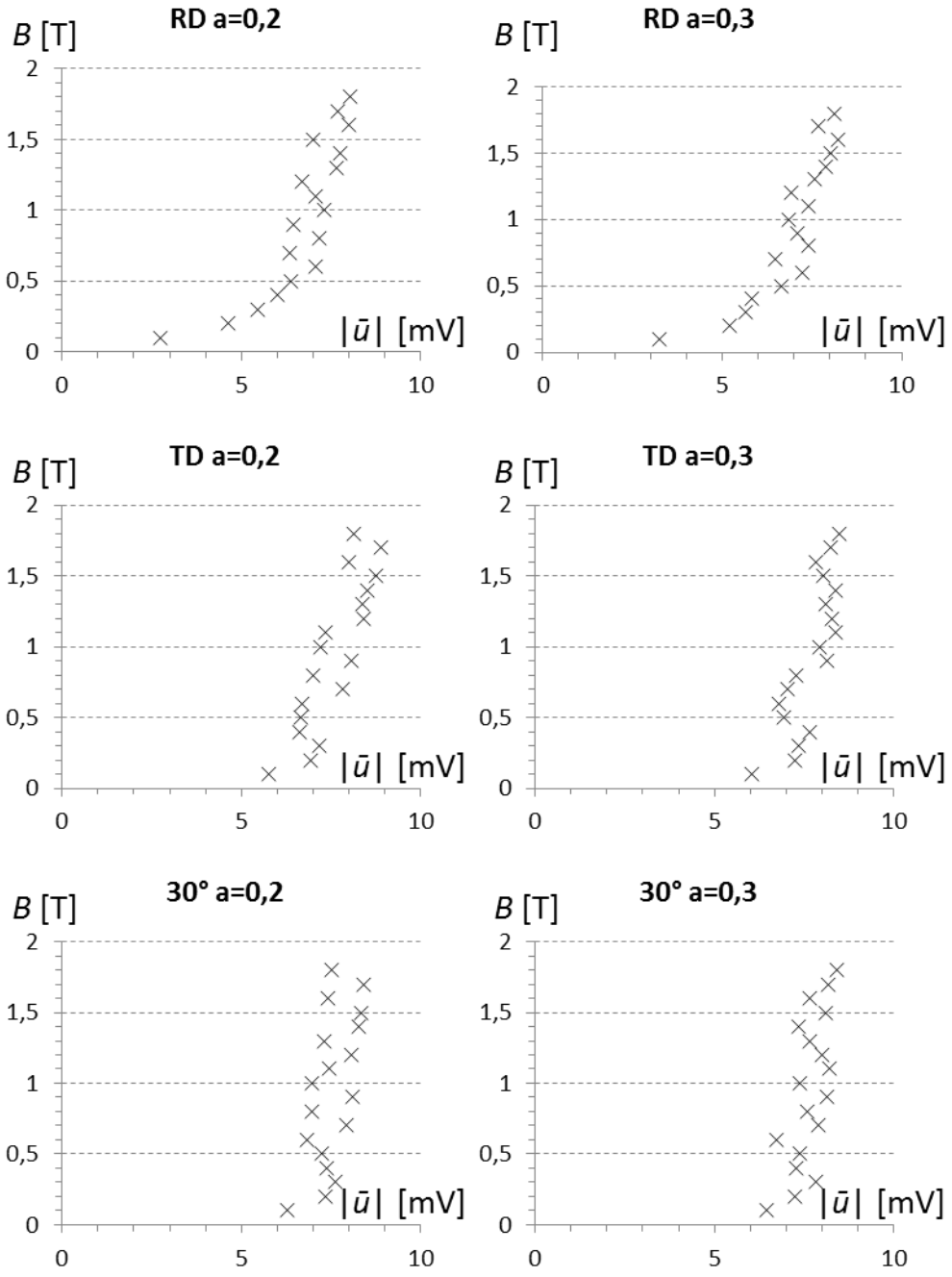

Figure 20 Examples of transfer curves for a nanocrystalline sensor of high width. The nominal induction value B (in T) is given as a function of the induced voltage u (in mV) in the windings of each strip. Case for a=0,2 is on the left side, case for a=0,3 on the right.

4 Verification of Sensors on a Model Transformer Core

The manufactured nanocrystalline sensors were verified using a three-legged, three-phase model transformer core. The material is the 23ZDKH90, the same high grain-oriented material used for calibration on the RSST. Dimensions of the core are 1m by 1m, with each leg 20cm wide and stacking height of 16mm.

The areas of the transformer core where I measured can be seen in Figure 21 below. Point A is in the so called T-Joint region of the core, which is the most interesting concerning rotational magnetization. Points B, and C are in the yoke and corner regions, respectively. Here again, it is expected that some form of RM can be detected. Lastly, point D is in the middle of the outer limb of the transformer core. It was chosen to compare with the results in the points A, B, and C, since at the point D no RM is expected. In fact, as mentioned earlier, the middle of the outer limb is often chosen to be a reference point, and sometimes the calibration curve is even recorded there.

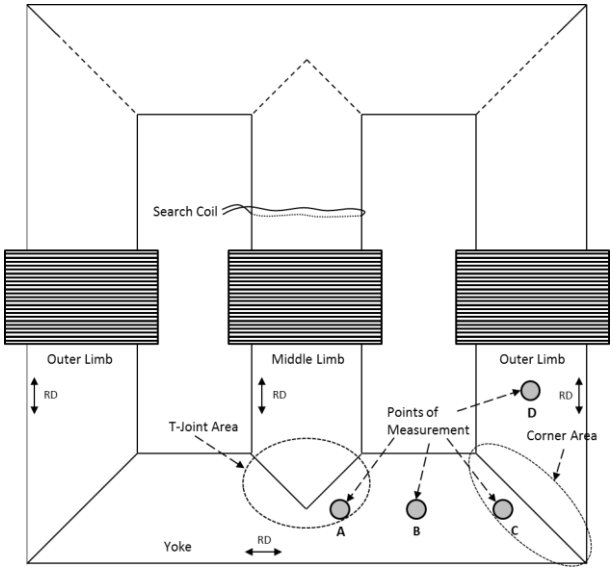

Figure 21 Model transformer core where the sensor transfer functions were verified.

Sensor values for all points were recorded at different levels of nominal *B*. In this case, nominal value of *B* was measured by a single pick-up coil around the middle limb of the transformer core.

Higher values of *B* were deliberately chosen, since the effectiveness of the former versions of the nanocrystalline sensor have already shown good results at lower levels of *B*. Another reason is that transformers are usually operating at or near saturation levels, standard value being 1,7T.

Detailed results are shown in Table 2. Overall, both sensors performed well at

	Sensor 1 (width 15mm)				Sensor 2 (width 10mm)			
Point	A	B	C	D	A	B	C	D
B_{NOM}	Difference form the nominal value of B given in %							
1,3T	-1,1	0,6	1,1	-21,1	-1,7	-1,7	-2,2	-19,4
1,5T	1,8	4,7	-4,7	-20,6	2,9	-5,9	0,0	-22,4
1,7T	-14,7	-10,7	-16,7	-25,3	-9,3	-20,0	-17,3	-28,0
1,8T	-11,5	-15,4	-23,8	-26,9	-9,2	-33,1	-30,8	-31,5

Table 2 Results of the sensor verification.

B_{NOM} values of 1,3T and 1,5T. At higher values of 1,7T and 1,8T; both sensors delivered values that were consistently lower than B_{NOM}. These results are partly in accordance with measurements performed with RSST, where at least the thinner sensor showed appearance of saturation, although at different levels.

Another interpretation of these results is that the measured induction really **is lower than** the nominal values at 1,7T and 1,8T. The fact that points A, B, and C, showed similar results, while point D constantly showed values that were lower than B_{NOM} seems to corroborate this assumption. Namely, due to the fact that point D is in the outer limb of the core, and the pick-up coil used for determining B_{NOM} was around the middle limb of the transformer core.

5 Simulation of the Nanocrystalline Sensors in RD and TD Directions

5.1 MACC

Simulation of the nanocrystalline sensors was performed using the MACC simulation tool, developed by our research group. MACC stands for "Multi-directionally non-linear magnetic equivalence circuit calculation" and was developed to numerically model transformer cores of Goss texture. Complex 2D and 3D models of single-phase, or three-phase transformer cores have been developed. For more about MACC, see [xxx].

For purposes of this thesis, simulation was built a fairly simple MACC model, using the methodology developed by my colleagues. It exists of (instead of simulating an entire transformer core) the equivalent circuit of just one lamination, which is represented by local elements (non-linear magnetic resistances) arranged in two directions, the rolling direction (RD), and the transverse direction (TD). Furthermore, two nanocrystalline sensors, represented by their corresponding local elements, are added "on top" of the lamination circuit. Last but not least, in order to take account for the interaction

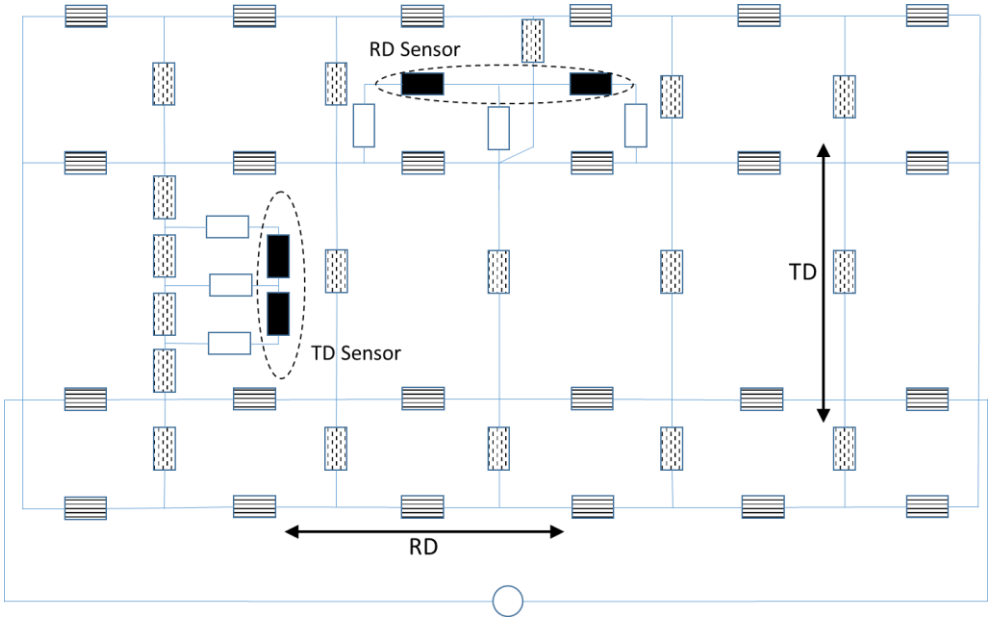

Figure 22 Equivalent circuit model with sensor.

between the lamination layer and the sensor layer, "connecting" resistances are added to the model. See Figure 22.

We can see four main flux paths (RD) and five transverse paths (TD), both represented by their corresponding resistances. Nanocrystalline sensors are shown in black and are positioned "on top" of the SiFe sheet. White resistances

take into account the magnetic interaction between the two layers, including the air gap introduced by the 50 μm thin copper wire.

The lamination part of the equivalent circuit is modelled after the same material used for the RSST probe, and for the three-phase model transformer used in measurements, namely highly grain oriented 23ZDKH90 which is laser scribed in the transverse direction. This material has very high anisotropy. Permeability values in RD and TD were measured, again using the RSST, and according to these values the non-linear magnetic resistances for the lamination part of the equivalent circuit have been set. Elements of the circuit which represent the nanocrystalline sensor have been taken from the catalogue.

5.2 Simulation Results

The results of the simulation can be seen in the figures below. They are shown in a different format then the previously presented measurement results. They show a time period of 20ms, which is equivalent to one period when the usual 50Hz alternating current excitation of the core is applied.

Two different geometries are presented. The first one is the 15mm wide sensor. In Figure 23, we can see that the RD sensor reaches saturation at around 1,2T which is consistent with the material properties, while the TD sensor shows a much lower flux density.

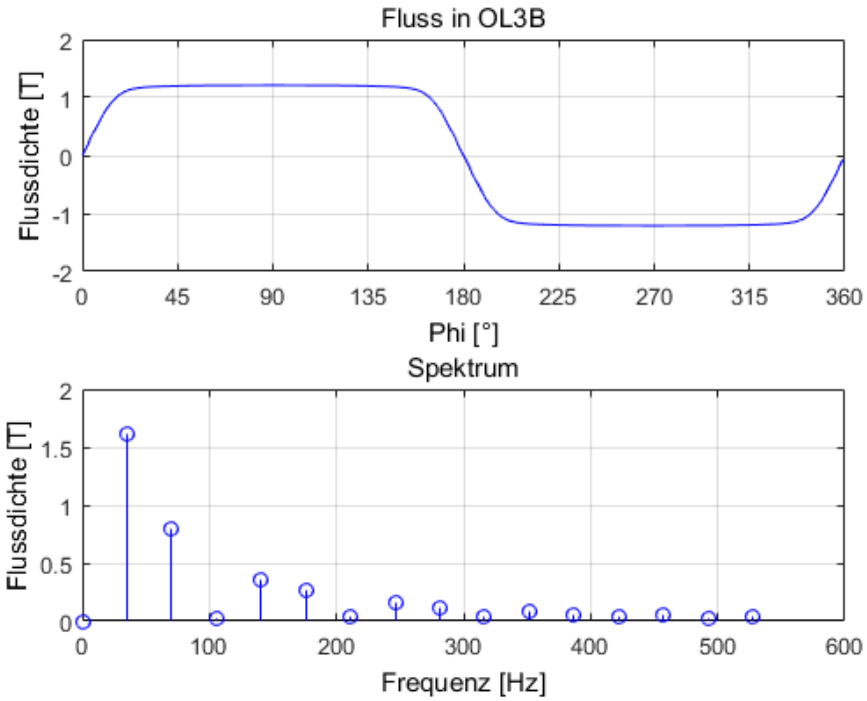

Figure 23 Magnetic induction in RD. Wide sensor.

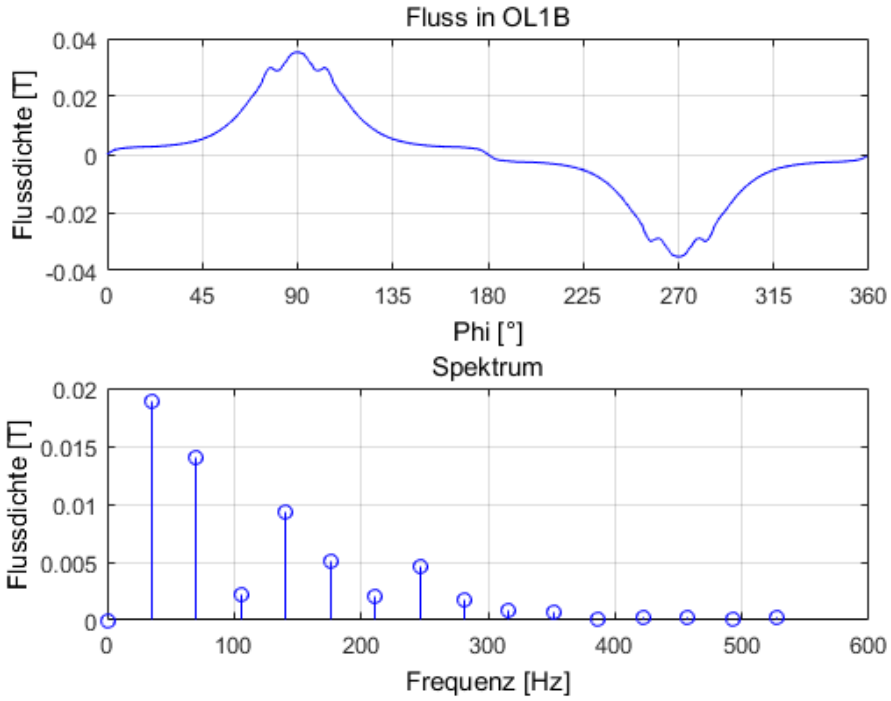

Figure 24 Magnetic induction in TD. Wide sensor.

The second one is the 10mm wide sensor. The results are similar to those of the wider sensor. However, it can be seen that the thinner sensor reaches saturation earlier than the wide one. This is in accordance with the measurements that were performed, which also show that the width of the sensor plays a role. The wider the sensor, the later the saturation is reached.

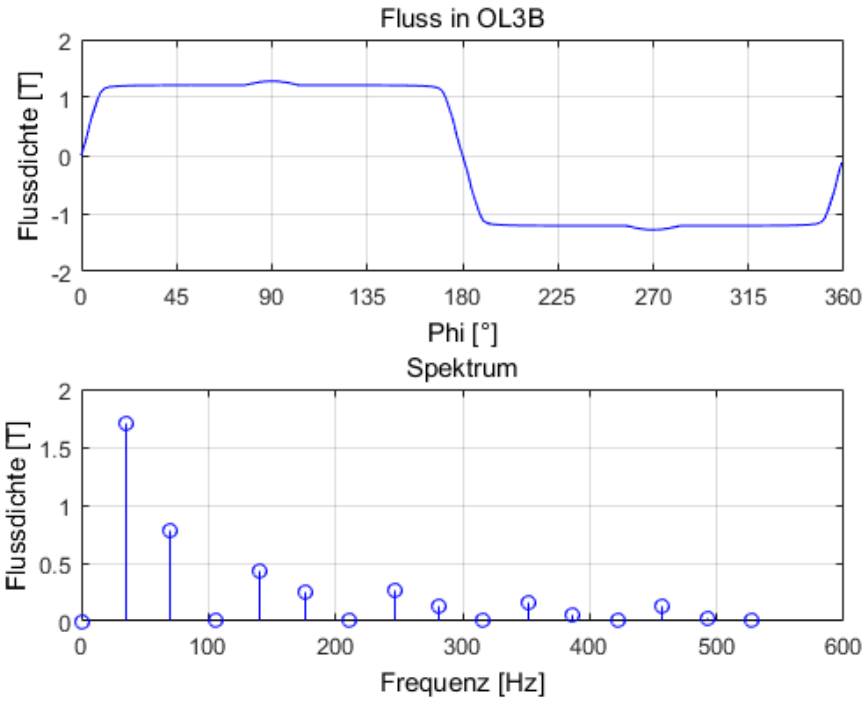

Figure 25 Magnetic induction in RD. Thinner sensor.

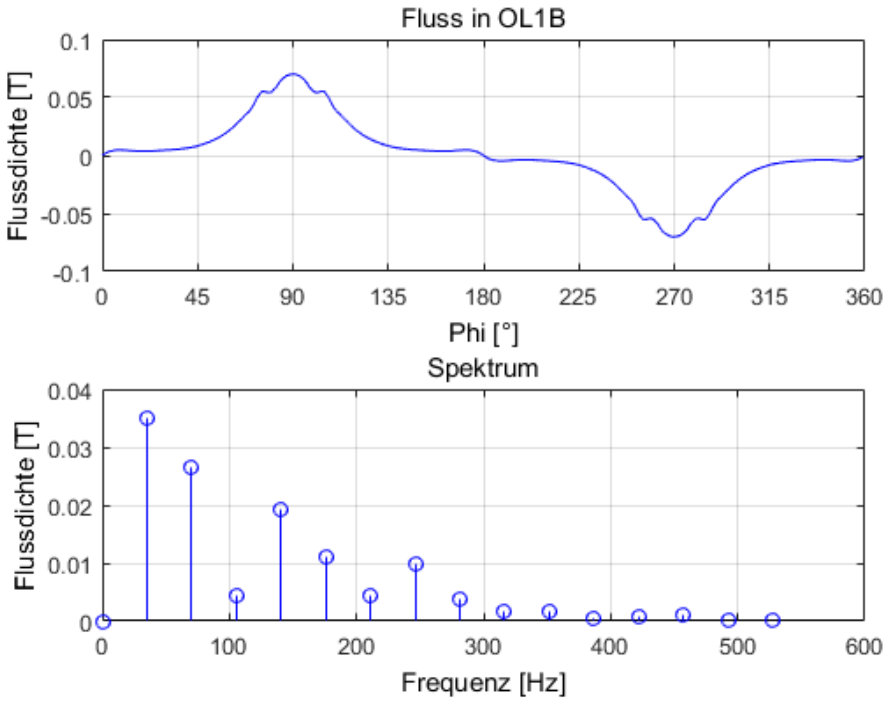

Figure 26 Magnetic induction in TD. Thinner sensor.

It should be pointed out that the MACC simulation cannot fully account for rotational magnetization at this time. This feature will be added in the future. Therefore, MACC simulation is to be seen as a representation of the nanocrystalline material in RD and TD in a transformer core with alternating magnetic induction.

6 Conclusions and Outlook

In the current work, a novel tangential induction sensor with a nanocrystalline ribbon as a core is developed and presented. Due to the excellent properties of the nanocrystalline sensor: low thickness, high permeability, zero magnetostriction, non-sensitivity to mechanical stress and relative high saturation magnetization, measurements within laminated cores are possible.

Magnetic induction sensors made out of nanocrystalline material have both disadvantages and advantages.

The most significant disadvantage we encountered was certainly the fact that this material is extremely brittle. Cutting it in a reliable fashion, so that one can manufacture identical sheets, has proven to be a very difficult, if not impossible task. This means that no two identical sensors, in fact not even identical sheets (ribbons) could be manufactured. This makes reproducibility somewhat challenging.

Another problem which has to do with the brittleness of the material is of course the fragility of a finished sensor. As mentioned earlier, it took several attempts to complete a particular sensor, regardless of the geometry in question. And even when this was accomplished, meaning the sensor was complete and intact, it then had to withstand the calibration process. As previously pointed out, calibrating the sensor using the RSST involved up to 100 measurements for each sensor.

The sensor was effectively tested in a three phase transformer core. The measurements in the rolling direction provide very promising results. Due to the high sensitivity of the sensor even for low nominal inductions, detection not only of the peak values, but also of the entire waveform of the local inductions are possible. The detection of the waveform enables the evaluation of the harmonics. However, measurements in transverse direction for evaluation of the rotational magnetization were not effective, due to the extreme high initial permeability of the nanocrystalline ribbon. For achieving this aim, a further optimization of the geometry of the nanocrystalline ribbon is necessary.

In order to further reduce the overall thickness of an interlaminar sensor, next steps are needed. Very promising in this respect is a project under way at our research group which aims to print 2-D sensors using a specially constructed 3D printer.

Acknowledgement

The Author thanks for support of the Austrian Science Fund FWF

(Project number P28481-N30)

References:

1 H. Pfützner, G. Shilyashki, P. Hamberger, M. Aigner, F. Hofbauer, M. Palkovits, G. Trenner, E. Gerstbauer, I. Matkovic, V. Galabov, "Automatic 3-D Building factor analyses of a grain-oreinted model transformer core," IEEE Trans.Magn. 50-4, 8400604, (2014).

2 F. Fauzi, D.M.M. Ahmad,"Normal direction of flux distribution in the mix 60° - 23° T-joint of three phase transformer cores," *Int.Pow.Eng.Conf.* Malaysia, pp. 570-572. (2010).

3 G. Shilyashki, H. Pfützner, P. Hamberger, M. Aigner, F. Hofbauer,

I. Matkovic, A. Kenov, „The impact of off-plane flux on losses and magnetostriction of transformer core steel," *IEEE Trans. Magn.*, 50-11, (2014).

4 H. Pfützner, E. Mulsalihovic, H. Yamaguchi, D. Sabic, G. Shilyashki, F. Hofbauer, "Rotatitional magnetization in transformer cores – a review," *IEEE Trans. Magn*. 47-11, pp. 4523-4533, (2011).

5 C. Ragusa, S. Zurek, C. Appino, A.J. Moses, "An intercomparison of rotational loss measurement in non-oriented Fe-Si alloys, " *J.Magn.Magn.Mat.* 320, pp.e623-e626, (2008).

6 G. Shilyashki, H. Pfützner, J. Anger, K. Gramm, F. Hofbauer, V. Galabov, E. Mulasalihovic, "Magnetostriction of transformer core steel considering rotational magnetization," *IEEE Trans. Magn*. 50-1, pp. 1-15 (2014).

7 D. Ahmad, F. Fauzi,"Influence of the mix 60° - 23 ° in different layers of T-joint of 3phase transformer core on longitudinal direction of flux distribution," *4th Int. P. Eng. and Opt. Conf. Malaysia*, pp. 566-569. (2010).

8 G. Loizos, D. Kefalas, A. Kladas, T. Souflaris, "Flux distribution analysis in three-phase Si-Fe Wound Transformer Cores", *IEEE Trans. Magn*. 46-2, pp. 594-597, (2010).

9 F. Marketos, D. Marnay, T. Ngnegueu,"Experimental and nummerical investigation of flux density distribution in the individual packets of a 100 kVA transformer cores", *IEEE Trans. Magn*. 48-4, pp. 1677-1680 (2010).

10 M. Belehosur, P. Marketos, A. Moses, J. Vincent, "Packet-to-packet variation of flux density in a three-phase, three-limb power transformer core," *IEEE Trans. Magn*. 46-2, pp. 642-645, (2010).

11 H. Pfützner, G. Shilyashki, Magnetic dummy sensors – A novel concept for interior flux distribution tests, *IJAEM* **48** (2015), 213-218.

12 G. Shilyashki, H. Pfützner, P. Hamberger, M. Aigner, E. Gerstbauer, M. Palkovits, G. Trenner," Pin Sensor for Interior Induction Measurements in Transformer Cores," IEEE Trans.Magn. 51-1, 4001904, (2015).

13 G. Shilyashki, H. Pfützner, P. Hamberger, M. Aigner, M. Palkovits, G. Trenner, E. Gerstbauer, Automatic 3-dimensional flux analyses of a 3-phase model transformer core, *IJAEM* **48** (2015), 277-281.

14 G. Shilyashki, H. Pfützner, M. Palkovits, P. Hamberger, M. Aigner, A tangential induction sensor for 3D-analyses of peripheral flux distributions in transformer cores, *IEEE Trans.Magn*. **51** (2014), 4003306.

15 G. Shilyashki, H. Pfützner "Nanocrystalline ribbons for induction measurements in laminated machine cores," *1&2-D Magn. Meas. & Test.* 16, OC-3, China, (2016)

16 http://www.vacuumschmelze.com/en/products/materials-parts/soft-magnetic/amorphous-nanocrystalline/vitroperm/vitroperm-physical-properties.html

17 A. Hasenzagl, B. Weiser, H. Pfützner, "Novel 3-phase excited single sheet tester for rotational magnetization", *J. Magn. Magn. Mater.*, vol. 160, pp. 180-182, 1996.

18 H. Pfützner, E. Mulasalihovic," Thin film technique for interior magnetic analysis of laminated machine cores," *Prz.Elektrot./ El.Rev. 85*, pp. 39-42 (2009).

19 B.D. Cullity, C:D. Graham, Introduction to Magnetic Materials, second edition, 2009, John Wiley & Sons, Inc.

20 D. Sabic, "Gleichfeld- und Dynamikeffekte auf elliptisch bzw. rhombisch rotierende Magnetisierung von anisotropen weichmagnetischen Materialien", (2011)., http://katalog.ub.tuwien.ac.at/AC07809349